Ocean Sci. Discuss., 10, 27–53, 2013
www.ocean-sci-discuss.net/10/27/2013/
doi:10.5194/osd-10-27-2013

Ocean Science Discussions

Oceanic dominance of interannual subtropical North Atlantic heat content variability

M. Sonnewald[1,2], **J. J.-M. Hirschi**[1], **and R. Marsh**[1]

[1]National Oceanography Centre Southampton, University of Southampton Waterfront Campus, European Way, Southampton SO14 3ZH, UK
[2]Institute for Complex Systems Simulation, University of Southampton, Southampton, SO17 1BJ, UK

Received: 30 November 2012 – Accepted: 23 December 2012 – Published: 10 January 2013

Correspondence to: M. Sonnewald (m.sonnewald@noc.soton.ac.uk)

Published by Copernicus Publications on behalf of the European Geosciences Union.

Abstract

Ocean heat content varies on a range of timescales. Traditionally the atmosphere is seen to dominate the oceanic heat content variability. However, this variability can be driven either by oceanic or atmospheric heat fluxes. To diagnose the relative contributions and respective timescales, this study uses a box model forced with output from an ocean general circulation model (OGCM) to investigate the heat content variability of the upper 800 m of the subtropical North Atlantic from 26° N to 36° N. The ocean and air-sea heat flux data needed to force the box model is taken from a 19 yr (1988 to 2006) simulation performed with the 1/12° version of the OCCAM OGCM. The box model heat content is compared to the corresponding heat content in OCCAM for verification. The main goal of the study is to identify to what extent the seasonal to interannual ocean heat content variability is of atmospheric or oceanic origin. To this end, the box model is subjected to a range of scenarios forced either with the full (detrended) ocean and air-sea fluxes, or their deseasoned counterparts. Results show that in all cases, the seasonal variability is dominated by the seasonal component of the air-sea fluxes, which produce a seasonal range in mean temperature of the upper 800 m of ∼ 0.42 °C. However, on longer timescales oceanic heat transport dominates, with changes of up to ∼ 0.30 °C over 4 yr.

The technique is subsequently applied to observational data. For the ocean heat fluxes, we use data from the RAPID program at 26° N from April 2004 to January 2011. At 36° N heat transport is inferred using a linear regression model based on the oceanic low-frequency transport in OCCAM. The air-sea flux from OCCAM is used for the period 2004 to 2006 when the RAPID timeseries and the OCCAM simulation overlap, and a climatology is used for the air-sea flux from 2006 onwards. The results confirm that on longer (> 2 yr) timescales the ocean dominates the ocean heat content variability, which is further verified using data from the ARGO project. This work illustrates that oceanic divergence significantly impacts the ocean heat content variability on timescales relevant for applications such as seasonal hurricane forecasts.

OSD

10, 27–53, 2013

1 Introduction

Globally, the equatorial region receives a surplus of energy from the sun. This surplus is redistributed through meridional heat transport (MHT) by the ocean and atmosphere (Kump et al., 1999; Bryden and Imawaki, 2001; Jayne and Marotzke, 2001). However, there is considerable spatial inhomogenity in this redistribution, expressed on the sea surface temperature variability. This surface temperature is used as a predictor for operational forecasts such as North American land falling tropical cyclones, European winters and the West African rainy season (Klotzbach, 2007; Scaife and Knight, 2008; Tompkins and Feudale, 2010). Locally, the heat content of a body of water is determined as the balance of the energy flux through its boundaries. Thus, if the boundary fluxes are known, the heat content can be determined. Baringer and Molinari (1999) and Warren (1999) describe how the energy transport (Q) through an oceanic section can be estimated as:

$$Q(x,z,t) = \int_{x_W}^{x_E}\int_{z}^{0} \rho c_p \theta(x,z,t) v(x,z,t) \mathrm{d}z\mathrm{d}x \quad (1)$$

The product of $\rho c_p \theta v$ is integrated over the area of a longitude-depth section (x_W and x_E stand for the zonal positions of western and eastern boundaries and the depth z), ρ is the in situ density, c_p the specific heat capacity per unit mass at constant pressure, θ the potential temperature referenced to the mean atmospheric pressure at mean sea level (1010 hPa), and v is the velocity component normal to the section. Thus, if estimating the transport in the North Atlantic, $\rho c_p \theta v$ is integrated across the depth and the width of the section. Variation in the heat content between two sections at different latitudes can stem from divergence of oceanic heat transport, or from heat exchange with the atmosphere. However, oceanic heat content (OHC) varies in response to both oceanic and atmospheric exchanges on shorter and longer (> 1 yr) timescales. Dong and Sutton (2005) suggest that the Atlantic Thermohaline Circulation is forced by the atmosphere, but that the timescale is set by the ocean.

OSD
10, 27–53, 2013

To assess the significance of the components of the oceanic MHT for OHC fluctuations, both observational and model data give valuable insights. Observational data have the benefit that they represent in situ oceanic values. However, limitations in spatial and temporal coverage can limit their usefulness. Ocean General Circulation Models (OGCMs) can give valuable insight as heat transport data can be retrieved from any location in the model grid at all times of a simulation. How accurately the model can represent the heat transport depends on factors such as the spatial resolution and the atmospheric forcing used (Marsh et al., 2009). However, at high resolutions an OGCM is computationally costly, and thus the forcing scenarios that can be tested are limited. One way to overcome this is to prescribe integral OGCM fluxes to computationally cheap box models. These can be forced with both observational and model data, as well as decompositions of the full MHT into their purely seasonal or interannual MHT components. Thus, their relative importance and effects can be assessed. Such box models can further be used to similarly analyze observational data. Similar work was done by Grist et al. (2010), who investigated the partitioning between the oceanic heat convergence and the air-sea heat flux. They found that the surface heat flux only played a small role in the interannual OHC variability away from the tropics.

The present study complements the Grist et al. (2010) study, developing a box model to specifically investigate the heat content variability of the subtropical North Atlantic (Sect. 2). This is defined as an 800 m deep ocean box from 26° N to 36° N corresponding to the depth of the Florida Strait. Firstly, using detrended data from the OCCAM model, the technique is verified by calculating the OHC using the box model, and comparing to the equivalent OHC variability in the OCCAM model. Having confirmed the method, the study goes on to investigate the sub- and interannual components of the oceanic and air-sea fluxes of heat to establish the relative importance of the ocean and atmosphere. This is repeated with detrended observational data from the RAPID project (Johns et al., 2011; Rayner et al., 2011; McCarthy et al., 2012). The results are presented in Sect. 3, followed by a discussion and concluding remarks in Sect. 4 with a focus on the origin of the signals.

OSD
10, 27–53, 2013

2 Data and methods

A heat budget box model analysis aproach is developed in this study. This was formulated in two ways. Firstly, we consider the volume transport in the upper 800 m looking at the advection of temperature with the volume flux (AV, the advective version in Sect. 2.2). Secondly, we consider the full-depth heat transport variability in a flux version of the model using the full-depth heat flux (FV, the flux version in Sect. 2.3). The following section describes how the box model versions are formulated and details the forcing used, which in the AV case was OGCM derived data and a mix of observational and OGCM data in the FV case.

2.1 OGCM and observational data

We use a 19 yr timeseries (1988 to 2006) from the eddy resolving 1/12° Ocean Circulation and Climate Advanced Model (OCCAM), a primitive equation, level-coordinate OGCM. OCCAM has high vertical resolution, with 66 levels, 14 of which are in the top 100 m. OCCAM was forced using a blend of National Center for Atmospheric Research (NCAR) reanalysis and satellite data (Coward and de Cuevas, 2005; Marsh et al., 2009).

The observational ocean transport data used in this study are from the RAPID-MOCHA project. Since April 2004 the RAPID-MOCHA observing system has been monitoring the Atlantic MOC at 26° N. The MOC is obtained by combining observations of the Florida Straits and Ekman transports, with a density driven recirculation (Hirschi et al., 2003; Cunningham et al., 2007; Kanzow et al., 2007; Johns et al., 2011; McCarthy et al., 2012). Data from the RAPID-MOCHA observing system are available from 3 April 2004 to the 1 Januar 2011.

OSD
10, 27–53, 2013

2.2 Advective version (AV) of the box model

Figure 1 illustrates the box model used to represent the top 800m of the subtropical North Atlantic between 26° N and 36° N. The oceanic heat content (OHC) is calculated using an Euler forward scheme:

$$\mathrm{OHC}_{t+1} = \mathrm{OHC}_t + \frac{\partial \mathrm{OHC}}{\partial t}\Delta t \tag{2}$$

$$\frac{\partial \mathrm{OHC}}{\partial t} = F_{26^\circ\mathrm{N}}(t) + F_{36^\circ\mathrm{N}}(t) + F_{\mathrm{AS}}(t) + F_{\mathrm{B}}(t) \tag{3}$$

Here $F_{26^\circ\mathrm{N}}$ and $F_{36^\circ\mathrm{N}}$ are timeseries of MHT, F_{AS} is the air-sea flux through the surface layer and F_{B} is the exchange through the bottom interface. From OCCAM we use timeseries of MHT from the upper 800 m from 26° N and 36° N available as 5-day averages from January 1988 to December 2006. The MHT timeseries for $F_{26^\circ\mathrm{N}}$ and $F_{36^\circ\mathrm{N}}$ are calculated as:

$$F_{26^\circ\mathrm{N}} = V_{26^\circ\mathrm{N}} T_{26^\circ\mathrm{N}} \rho c_p \tag{4}$$

$$F_{36^\circ\mathrm{N}} = V_{36^\circ\mathrm{N}} T_{36^\circ\mathrm{N}} \rho c_p \tag{5}$$

where $V_{26^\circ\mathrm{N}}$ and $V_{36^\circ\mathrm{N}}$ are the volume transports through longitude-depth sections at 26° N and 36° N down to a depth of 800 m. $T_{26^\circ\mathrm{N}}$ and $T_{36^\circ\mathrm{N}}$ are the average temperatures at the southern (26° N) and northern (36° N) interfaces of the box. $V_{26^\circ\mathrm{N}}$, $V_{26^\circ\mathrm{N}}$, $T_{26^\circ\mathrm{N}}$ and $T_{36^\circ\mathrm{N}}$ were retrieved from the OGCM.

To calculate the exchange through the bottom interface (F_{B}) we use the relationship between the volumes ($V_{26^\circ\mathrm{N}}$ and $V_{36^\circ\mathrm{N}}$) entering and leaving the sides of the section, and thus determining the direction and magnitude of the heat flux F_{B} according to:

$$F_{\mathrm{B}}(t+1) = \begin{cases} -(V_{26^\circ\mathrm{N}} - V_{36^\circ\mathrm{N}}) T_{\mathrm{interface}}(t) \rho c_p & \text{if} \quad V_{26^\circ\mathrm{N}} > V_{36^\circ\mathrm{N}} \\ (V_{26^\circ\mathrm{N}} - V_{36^\circ\mathrm{N}}) T_{\mathrm{interface}}(t) \rho c_p & \text{if} \quad V_{26^\circ\mathrm{N}} < V_{36^\circ\mathrm{N}} \end{cases} \tag{6}$$

OSD
10, 27–53, 2013

where $T_{\text{interface}}$ was retrieved from the OCCAM model. The air-sea flux field was retrieved from OCCAM for the area of F_{AS}. See Fig. 2 (left panels) for time series of the various forcing data used in AV.

Throughout the study, we focus on the variability, working with detrended fluxes where the time mean is removed. Furthermore, for the first timestep, the OHC is calculated with a set of initial values retrieved from OCCAM. For subsequent timesteps, the temperature (T) of the ocean box is calculated using the volume (V, kept fixed at $5.4 \times 10^{15}\,\text{m}^3$ and estimated from OCCAM) of the ocean box, the average density ($\rho = 1025\,\text{kg}\,\text{m}^{-3}$) and the specific heat capacity ($c_p = 3850\,\text{J}\,\text{kg}^{-1}\,\text{K}^{-1}$):

$$T(t) = \frac{\text{OHC}(t)}{V \rho c_p} \tag{7}$$

2.3 Flux version (FV) of the box model

For the FV of the box model we use the RAPID data from 26° N. As only the full depth integrated transport is available from RAPID, the FV of the box model reflects this by assuming that any net transport acts to increase the OHC in the surface box, as opposed to mixing happening through an F_{B} term:

$$\frac{\partial \text{OHC}}{\partial t} = F^*_{26^\circ\text{N}}(t) + F^*_{36^\circ\text{N}}(t) + F_{\text{AS}}(t) \tag{8}$$

The air-sea flux is identical to that used in AV, while the ocean heat fluxes at 26° N and 36° N are the net heat fluxes over the entire section from the surface to the sea floor. The RAPID observational data at 26° N are used to calculate $F^*_{26^\circ\text{N}}$. Here, the meridional overturning circulation (MOC) is converted to MHT as in Johns et al. (2011):

$$\text{MHT(PW)} = 0.079\text{MOC} + 0.12\text{PW} \tag{9}$$

No observational MHT estimate exists for 36° N. However, as Grist et al. (2009) and Josey et al. (2009) demonstrate, there is a strong meridional coherence of the MOC in

OSD
10, 27–53, 2013

the study area. This was exploited, and $F^*_{36^\circ N}$ is obtained using the relationship between the transport at 26° N and 36° N in the OCCAM derived data, together with the overall lag between the two latitudes. However, a strong linear relationship is not immediately evident between the MHT at 26° N and 36° N in OCCAM (Fig. 3, blue curve). To determine a more robust relationship between 26° N and 36° N we used a low-frequency filter (cut-off 3.7 cycles yr^{-1}), and obtain an increased correlation (Fig. 3, red curve). We further account for the time lag between MHT fluctuations between the two latitudes, such that maximum correlation arises between MHT at 36° N and 15 days earlier at 26° N. We thus arrived at the linear low pass model:

$$F^*_{36^\circ N} = 1.57 \times 10^{-3} + 0.682 \times F^*_{26^\circ N} \quad (10)$$

However, the regression model does not account for the time lag between the two latitudes, which was determined to be of the order of 15 days. Thus, this was added to the regression model to obtain $F^*_{36^\circ N}$.

Thus, we used the AV and FV box models together with their respective observation and model derived forcing to determine the OHC variability in the 800 m surface box. However, the observational data used full depth integrated forcing, assuming variability would express itself in the surface region. To investigate the seasonal component of the heat transport, climatologies were constructed using a simple arithmetic mean of five-day segments as in Atkinson et al. (2010). The interannual component was determined by estimating the residual of the forcing data with the seasonal signal subtracted ($MHT_{interannual} = MHT - MHT_{Clim}$).

3 Results

As a first step, we present the full fluxes used to force the model. We validate the advective and flux versions of the box model (AV and FV, respectively). This is followed by a series of experiments where the box model is subjected to different forcing scenarios.

OSD
10, 27–53, 2013

3.1 Heat fluxes

Figure 2 illustrates the heat fluxes used to force the AV and FV box models. Table 1 shows the variability, minimum and maximum heat transport. The air-sea flux dominates the statistics, while the model forcing was found to be smaller and less variable overall than the observational forcing. The surface flux was seen to have a net cooling effect, while the combined oceanic effect was a net warming, i.e. the MHT at 26° N was found to be larger than at 36° N. This difference in heat transport is expected as heat is lost to the atmosphere. The climatological air-sea flux shows a relatively smooth seasonal cycle. In contrast, particularly the observational oceanic climatologies do not seem to fully capture the seasonal signal (Fig. 2), which could leave a seasonal signal in the interannual forcing. This was confirmed by spectral analysis. The timing of maximum heat transport was found in June to November and minimum found in January to March in the observational transports, as reported by Johns et al. (2011) and Atkinson et al. (2010). These maximum and minimum transports are similar both at 26° N and 36° N. At 26° N maximum transport occurs between late July and November, while minimum transports occur between mid February and mid March. At 36° N, maximum transport occurs from mid August to October and minimum transport occurs from March to April. In both cases the amplitude of the seasonal signal at 36° N is smaller than at 26° N, as demonstrated in table 1, suggesting that the seasonality becomes less pronounced further away from the equator in agreement with studies such as Jayne and Marotzke (2001); Fasullo and Trenberth (2008).

3.2 Model validation

OHC estimates from the two box-model formulations AV and FV are now compared to the OHC variability in OCCAM. For convenience we convert OHC into temperature according to Eq. (7) and in the remainder of the paper OHC will be quantified in terms of the average temperature of the subtropical North Atlantic box.

OSD
10, 27–53, 2013

The AV of the box model is seen in Fig. 4 to largely reproduce the OHC variability of the OCCAM model. Figure 5 shows the interannual component of the OHC variability. This further illustrates that the AV box model captures the variability reasonably well. Three major peaks are visible in both AV and OCCAM, together with a sharp peak. Broad OHC maxima occur in the early and mid 1990s as well as between 2003 and 2005, wheras a short lived maximum is found in 1999. The timing of the OHC variability is also consistent at higher frequencies. The agreement between OCCAM and the box model is not as good for the second formulation FV where the assumtions made are tested by forcing the FV box model using MHT from the OCCAM model at 26° N and 36° N. However, the FV still captures the OHC variability reasonably well, as demonstrated in Fig. 4. Figure 5 illustrates that it overestimates the OHC peak in the early 1990s and the following trough. However, good agreement is generally found after that: FV accurately captures the sharp peak in 1999 and the trough in 2006 as well as the maxima in the mid 1990s and mid 2000s. Overall, Fig. 5 confirms that both AV and FV of the box model capture the variability in OHC in OCCAM reasonably well, with the AV box model interannual OHC median deviation from the OCCAM model of -7.7×10^{-3} °C (standard deviation: 5.7×10^{-2} °C), and box model FV 2.4×10^{-2} °C (standard deviation: 0.1 °C). This agreement suggests that the box model can be applied to investigate the sub- and interannual components of the oceanic and air-sea contributions to HC variability.

3.3 Box model results

Figure 6a illustrates the results of the AV box model forced with OCCAM derived MHT. The seasonality in the OHT contributes very little to the overall seasonal OHC signal, and remains close to zero. The overall seasonal signal for the OHC corresponds to a mean seasonal temperature range of ∼0.42 °C which is mainly due to the air-sea fluxes. The interannual signal can be seen again to have three broad OHC maxima as well as the sharp 1999 peak. Most of the variability in the interannual signal is accounted for by the oceanic MHT which also has the three broad peaks and one sharp

OSD
10, 27–53, 2013

peak. The interannual atmospheric variability can be seen to affect the amplitude of the signal, but overall the oceanic heat transport dominates. The same pattern is also found in the box model FV. Figure 6b shows the results from the FV box model, illustrating that the amplitude of the seasonal signal (~ 0.45 °C) is again dominated by the atmosphere, but is amplified slightly by the ocean whose contribution is larger than in the AV case. As before, the interannual signal is dominated by the ocean. Unfortunately, the effect of the atmosphere can only be assessed to the end of 2006, since the air-sea fluxes from OCCAM are not available beyond 2006. However, the available timeline suggests that the interannual variability of the atmosphere has a smaller effect in the FV case, changing the amplitude of the overall interannual signal only sightly.

To visualise the timescales over which the oceanic and atmospheric components of OHC tendency act and their respective magnitude and variability, key statistics are displayed in Fig. 7. Here, a sliding window technique is used to collect the maximum amplitude of temperature change within windows of prescribed length. Sliding the window along the timeseries allows us to collect the median, first and third quartiles of peak-to-peak temperature variability. Shown are the median (solid coloured line) first and third quartiles (respectively lower and upper bound of coloured area) for the absolute magnitude ($|\Delta T|$) of OHC change for time windows ranging from 5 days up to 4 yr. Figure 7a illustrates that in AV over 6 months, the seasonal atmospheric component changes OHC by 0.42 °C, while the seasonality of ocean heat transport only changes the temperature by 0.02°C. However, over 4 yr the interannual oceanic component can contribute 0.3 °C, while the interannual atmospheric component contributes only 0.1 °C. Further, the overall OHC variability follows the seasonal atmosphere closely up to 6 months. The OHC change due to the interannual oceanic component steadily increases as the window length is increased. This confirms the dominance of the ocean on interannual timescales compared to the much smaller influence of interannual atmospheric variability. Figure 7b shows the same pattern. The overall OHC variability does not follow the seasonal atmosphere as closely, but a clear levelling after 6 months

OSD
10, 27–53, 2013

is observed, while the same partitioning between the ocean and atmosphere is seen on sub- to interannual timescales.

To further assess the performance of the two box model versions we compare these to observations of OHC anomalies from the ARGO project using the gridded dataset by Ivchenko et al. (2010), Fig. 8. Unfortunately, the section from 26 to 36° N was not available, but neighbouring latitudinal bands from 20 to 30° N (stippled) and 30 to 40° N (solid) are thought to give a reasonable approximation, along with the mean (bold solid). These illustrate that the interannual variability is reasonably well captured using AV, and also with FV. This further supports the importance of the oceanic origin of OHC variability as the FV box model uses observational ocean data while AV relies on data from OCCAM which has been forced with atmospheric reanalysis data. The ARGO data is seen to have larger variability than the box model data. However, both AV and FV can be seen to show general trends that are similar to those seen in ARGO. Overall, in both the ARGO and box model data the period from 1999 to December 2010 is seen to start with a decrease, followed by two periods of increased OHC between 2002 and 2005, and from mid 2006 to mid 2008. It is noteworthy that the decrease in OHC seen in the Argo data from mid 2008 to 2010 is clearly visible in the box model results. In Argo this decrease is particulary sharp for the 30° N to 40° N band and coincided with a marked reduction of the MOC during that period (McCarthy et al., 2012).

4 Discussion

The assumptions underpinning a box model of the subtropical North Atlantic heat balance are tested by comparing the box model temperature to a mean temperature in the equivalent volume of an eddy-resolving OGCM (OCCAM). Figure 4 reveals the extent of the mismatch, highlighting that OCCAM has a smaller reasonal cycle. The larger signal in the box model could suggest either a shortcoming in the box model, or in the model derived MHT. However, a highly significant correlation at the 99 % level was found (correlation 0.91 with 51 degrees of freedom) between the box model

OSD
10, 27–53, 2013

and OCCAM temperature evolution. Furthermore, the frequency spectra of the non-seasonal full OCCAM and the box model non-seasonal transports were compared. These demonstrated that the atmospheric contribution to the non-seasonal transport is small, and that the oceanic non-seasonal transport can account for the significant peaks both in OCCAM and the box model. This suggests that the box model approach is valid for looking at cases where the time mean heat transport is removed. This is confirmed using OHC anomalies from ARGO data, illustrating that FV captures observed OHC anomaly variability. However, some discrepancy is is found between advective (AV) and flux (FV) versions of the box model. Neither version takes horizontal or vertical mixing into account, which can likely account for much of the discrepancy. A further source of error could be the five day averaging of output variables in the OCCAM model. This leads to underestimating the eddy correlation, and any variable varying significantly within the five day window (Huerta-Casas and Webb, 2012). However, the smaller OCCAM seasonal signal suggests a seasonality in the "missing" flux, which would be suprising in the presumably more chaotic sum of eddy correlations. Determining the source of this heat flux is outside the scope of this study.

We observe a cooling from mid 1991 to 1994 in the AV model forced case, Fig. 6a. This could be attributed to the June 1991 eruption of Mt. Pinatubo, which caused a reduction in radiative forcing of $2.4\,\mathrm{W\,m^{-2}}$ (Feulner and Rahmstorf, 2010) and is also visible in observation based reconstructions of global sea surface temperatures such as Domingues et al. (2008). In our model, the cooling signal is only attributed to interannual oceanic HT. Kanzow et al. (2010) suggests that the annual variability in the RAPID MHT is caused by variations in the geostrophic circulation. Thus, the interannual temperature variability could be attributed to changes in the pressure gradient. In OCCAM mass transport, patterns similar to the non-seasonal temperature evolution can be seen in the interannual component of the depth and longitudinally integrated baroclinic transport (Hirschi et al., 2007). The baroclinic component of the transport is a result of zonal density and pressure gradients. These could thus be one of the main driving forces giving rise to the non-seasonal temperature variability.

OSD
10, 27–53, 2013

Like Grist et al. (2010), we found a good agreement between modelled and observational OHC in the subtropical North Atlantic. However, this study used data from the eddy resolving 1/12° OGCM, where Grist et al. (2010) used an eddy permitting 1/4° OGCM. Further, we affirm the conclusions from the model driven case with observations, finally performing an independent verification using ARGO data. Grist et al. (2010) look beyond the subtropical North Atlantic, investigating the region from 22° N to 65° N. They found that the interannual signal in OHC variability is largely ocean dominated in the subtropics and subpolar regions, but increasingly dominated by atmospheric (surface flux) variability towards the tropics. We suspect our AV box model would confirm these results, but they would be difficult to confirm using a similar FV box model. The ocean fluxes at the northern boundary of such a tropical box would be given by the RAPID-MOCHA observations. However, low meridional coherence of the MOC (and therefore of the MHT) in the Tropics makes the inference of the ocean fluxes at the southern boundary of the box difficult.

The ARGO data is seen to have larger variability than the box model data. This could be a reflection of the larger region considered in the ARGO data, however, it could also reflect a surface damping effect resulting from the use of a reanalysis product to force the OCCAM GCM, where the surface forcing for the AV and FV box models was retrieved. The reanalysis data used to force the OCCAM GCM (Marsh et al., 2009) uses an atmospheric model guided by available data and surface ocean fields. Thus, due to the one way communication across the ocean-atmosphere interface, feedbacks and possible amplifications will be damped. Furthermore, spatial and temporal smoothing could also potentially lead to damping of the atmospheric signal.

5 Conclusions

Understanding the underlying mechanisms driving oceanic heat content variability are potentially of great socioeconomic importance, as these can feed back onto the atmosphere and affect the climate. However, changes in temperature will most likely not

OSD
10, 27–53, 2013

occur homogeneously across the ocean box, but be of a more localized nature. Such local temperature changes can have much larger amplitudes. In this context, the effect of the non-seasonal ocean is of particular interest. This is because its large interannual variability makes it less predictable than the seasonal air-sea flux. We have illustrated the relative importance of the ocean and air-sea flux on the OHC variability in the subtropical North Atlantic. Using both purely model derived data, as well as observational data, we have shown that the ocean dominates the interannual subtropical OHC variability in the Atlantic, while the air-sea flux dominates the seasonal variability. The short duration of the observational record inhibited the isolation of the seasonal signal. However, we show that the atmosphere dominates the shorter (seasonal and shorter) timescales, while the ocean dominates interannual timescales. Anomalous ocean MHT may therefore contribute to the development of anomalous upper ocean heat content and SSTs in the subtropical Atlantic with potential feedback on the atmosphere (e.g. hurricane activity). We note that the build-up of heat in the mid-2000s was coincident with a gradual increase in the number of major Hurricanes during that period culminating in the active hurricane season of 2004. This was followed by the record season of 2005 which also coincided with a sharp OHC increase during that year. Finally, above average Hurricane activity was also recorded in 2008 which again coincided with high OHC values (Mainelli et al., 2008; Grossmann and Morgan, 2011; Hoyos et al., 2006). However, Hurricanes are sensitive to sea surface temperatures rather than directly to OHC, and the causal link between OHC and SST development needs further study.

Acknowledgements. We thank Andrew Coward for providing output from the OCCAM OGCM. Data from the RAPID-WATCH MOC monitoring project are funded by the Natural Environment Research Council and are freely available from www.noc.soton.ac.uk/rapidmoc. Further thanks to Peggy Courtois and Vladimir Ivchenko (Ivchenko et al., 2010) for help with the ARGO comparison.

OSD
10, 27–53, 2013

References

Atkinson, C. P., Bryden, H. L., Hirschi, J. J-M., and Kanzow, T.: On the seasonal cycles and variability of Florida Straits, Ekman and Sverdrup transports at 26° N in the Atlantic Ocean, Ocean Sci., 6, 837–859, doi:10.5194/os-6-837-2010, 2010. 34, 35

Baringer, M. O. and Molinari, R.: Atlantic Ocean baroclinic heat flux at 24 to 26° N, Geophys. Res. Lett., 26, 353–356, 1999. 29

Bryden, H. L. and Imawaki. S.: Ocean heat transport, in: Ocean Circulation and Climate, edited by: Siedler, G., Church, J., and Gould, J., London, Academic Press, 455–474, 2001. 29

Coward, A. C. and de Cuvas, B. A.: The OCCAM 66 level model: physics, initial conditions and external forcing, SOC internal report, No. 99, 2005. 31

Cunningham, S. A., Kanzow, T., Rayner, D., Baringer, M. O., Johns, W. E., Marotzke, J., Longworth, H. R., Grant, E. M., Hirschi, J. J.-M., Beal, L. M., Meinen, C. S. and Bryden, H. L.: Temporal variability of the Atlantic meridional overturning circulation at 26.5° N, Science, 317, 935–938, doi:10.1126/science.1141304, 2007. 31

Domingues, C. M., Church, J. A., White, N. J., Gleckler, P. J., Wijffels, S. E., Barker, P. M., and Dunn, J. R.: Improved estimates of upper-ocean warming and multi-decadal sea-level rise, Nature, 453, 1090–1093, 2008. 39

Dong, B. and Sutton, R. T.: Mechanism of interdecadal thermohaline circulation variability in a coupled ocean–atmosphere GCM, J. Climate, 18, 1117–1135, 2005. 29

Fasullo, J. T. and Trenberth, K. E.: The annual cycle of the energy budget, Part II: Meridional structures and poleward transports, J. Climate, 21, 2313–2325, 2008. 35

Feulner, G. and Rahmstorf, S.: On the effect of a new grand minimum of solar activity on the future climate on Earth, Geophys. Res. Lett., 37, L05707, doi:10.1029/2010GL042710, 2010. 39

Grossmann, I. and Morgan, M. G.: Tropical cyclones, climate change, and scientific uncertainty: what do we know, what does it mean, and what should be done? Climatic Change, 108, 543–579, 2011. 41

Grist, J. P., Marsh, R., and S. A. Josey, S. A.: On the relationship between the North Atlantic meridional overturning circulation and the surface-forced overturning stream function, J. Climate, 22, 4989–5002, doi:10.1175/2009JCLI2574.1, 2009. 33

Grist, J. P., Josey, S. A., Marsh, R., Good, S. A., Coward, A. C., de Cuevas, B. A., Alderson, S. G., New, A. L., and Madec, G.: The roles of surface heat flux and ocean heat transport

OSD
10, 27–53, 2013

convergence in determining Atlantic Ocean temperature variability, Ocean Dynam., 60, 771–790, doi:10.1007/s10236-010-0292-4, 2010. 30, 40

Hirschi, J. J.-M., Baehr, J., Marotzke, J., Stark, J., Cunningham, S., and Beismann, J.-O.: A monitoring design for the Atlantic meridional overturning circulation, Geophys. Res. Lett., 30, 1413, doi:10.1029/2002GL016776, 2003. 31

Hirschi, J. J.-M., Killworth, P. D., and Blundell, J. R.: Subannual, seasonal, and interannual variability of the North Atlantic meridional overturning circulation, J. Phys. Oceanogr., 37, 1246–1265, 2007. 39

Hoyos, C. D., Agudelo, P. A., Webster, P. J., and Curry, J. A.: Deconvolution of the factors contributing to the increase in global hurricane intensity, Science, 312, 94–97, 2006. 41

Huerta-Casas, A. M. and Webb, D. J.: High frequency fluctuations in the heat content of an ocean general circulation model, Ocean Sci., 8, 813–825, doi:10.5194/os-8-813-2012, 2012. 39

Ivchenko, V. O., Wells, N. C., Aleynik, D. L., and Shaw, A. G. P.: Variability of heat and salinity content in the North Atlantic in the last decade, Ocean Sci., 6, 719–735, doi:10.5194/os-6-719-2010, 2010. 38, 41

Jayne, S. R. and Marotzke, J.: The dynamics of ocean heat transport variability, Rev. Geophys., 39, 385–411, 2001. 29, 35

Johns, W., Bryden, H., Baringer, M., Beal, L., Cunningham, S., Kanzow, T., Hirschi, J., Marotzke, J., Garraffo, Z., Meinen, C., and Curry, R.: Continuous, array-based estimates of Atlantic Ocean heat transport at 26.5° N, J. Climate, 24, 2429–2449, doi:10.1175/2010JCLI3997.1, 2011. 30, 31, 33, 35

Josey, S. A., Grist, J. P., and Marsh, R.: Estimates of meridional overturning circulation variability in the North Atlantic from surface density flux fields, J. Geophys. Res., 114, C09022, doi:10.1029/2008JC005230, 2009. 33

Kanzow, T., Cunningham, S., Rayner, D., Hirschi, J., Johns, W. E., Baringer, M., Bryden, H., Beal, L., Meinen, C., and Marotzke, J.: Flow compensation associated with the meridional overturning circulation, Science, 317, 938–941, doi:10.1126/science.1141293, 2007. 31

Kanzow, T., Cunningham, S., Johns, W. E., Hirschi, J. J.-M., Marotzke, J., Baringer, M., Meinen, C., Chidichimo, M. P., Atkinson, C., Bryden, H., and Collons, J.: Seasonal variability of the Atlantic meridional overturning circulation at 26.5° N, J. Climate, 23, 5678–5698, doi:10.1175/2010JCLI3389.1, 2010. 39

OSD
10, 27–53, 2013

Klotzbach, P. J.: Recent developments in statistical prediction of seasonal Atlantic basin tropical cyclone activity, Tellus A, 59, 511–518, 2007. 29

Kump, L. R., Kasting, J. F., and Crane, R. G.: The Earth System, Upper Saddle River, Prentice Hall, NJ, 1999. 29

Lyman, J. M., Good, S. A., Gouretski, V. V., Ishii, M., Johnson, G. C., Palmer, M. D., Smith, D. M., and Willis, J. K.: Robust warming of the global upper ocean, Nature, 465, 334–337, 2010.

Mainelli, M., Demaria, M., Shay, L. K., and Goni, G.: Application of oceanic heat content estimation to operational forecasting of recent atlantic category 5 hurricanes, Weather Forecast., 23, 3–16, 2008. 41

Marsh, R., de Cuevas, B. A., Coward, A. C., Jacquin, J., Hirschi, J. J.-M., Aksenov, Y., Nurser, A. J. G., and Josey, S. A.: Recent changes in the North Atlantic circulation simulated with eddy-permitting and eddy-resolving ocean models, Ocean Model., 28, 226–239, 2009. 30, 31, 40

McCarthy, G. D., Frajka-Williams, E., Johns, W. E., Baringer, M. O., Meinen, C. S., Bryden, H. L., Rayner, D., Duchez, A., Roberts, C. D., and Cunningham, S. A.: Observed interannual variability of the Atlantic meridional overturning circulation at 26.5° N, Geophys. Res. Lett., 39, L19609, doi:10.1029/2012GL052933, 2012. 30, 31, 38

Rayner, D., Hirschi, J. J.-M., Kanzow, T., Johns, W. E., Wright, P. G., Frajka-Williams, E., Bryden, H. L., Meinen, C. S., Baringer, M. O., Marotzke, J., Beal, L. M., and Cunningham, S. A.: Monitoring the Atlantic meridional overturning circulation, Deep Sea-Res. Pt. II, 58, 1744–1753, doi:10.1016/j.dsr2.2010.10.056, 2011. 30

Scaife, A. A. and Knight, J. R.: Ensemble simulations of the cold European winter of 2005–2006, Q. J. Roy. Meteor. Soc., 134, 1647–1659, 2008. 29

Tompkins, A. M. and Feudale, L.: Seasonal ensemble predictions of West African monsoon precipitation in the ECMWF System 3 with a focus on the AMMA special observing period in 2006, Weather Forecast., 25, 768–788, doi:10.1175/2009WAF2222236.1, 2010. 29

Warren, B. A.: Approximating the energy transport across oceanic sections, J. Geophys. Res., 104, 7915–7920, 1999. 29

OSD

10, 27–53, 2013

Table 1. Table of minimum, maximum (PW) and variance (PW^2) values of the heat transports used (detrended and with the mean removed) for the AV (OCCAM) and FV (RAPID) of the box model. Northward (ocean) and downwards (air-sea) transports are positive.

Forcing	Min	Max	Var
F_{AS}	−1.76	1.05	0.50
$F_{26^\circ N}$	−1.20	0.99	0.076
$F_{36^\circ N}$	−1.17	1.15	0.12
$F^*_{26^\circ N}$	−1.18	1.17	0.14
$F^*_{36^\circ N}$	−0.80	0.80	0.064
F_{AS} clim.	−1.20	0.90	0.47
$F_{26^\circ N}$ clim.	0.80	1.28	0.013
$F_{36^\circ N}$ clim.	0.57	1.08	0.015
$F^*_{26^\circ N}$ clim.	−0.42	0.36	0.044
$F^*_{36^\circ N}$ clim.	−0.25	0.27	0.064

OSD
10, 27–53, 2013

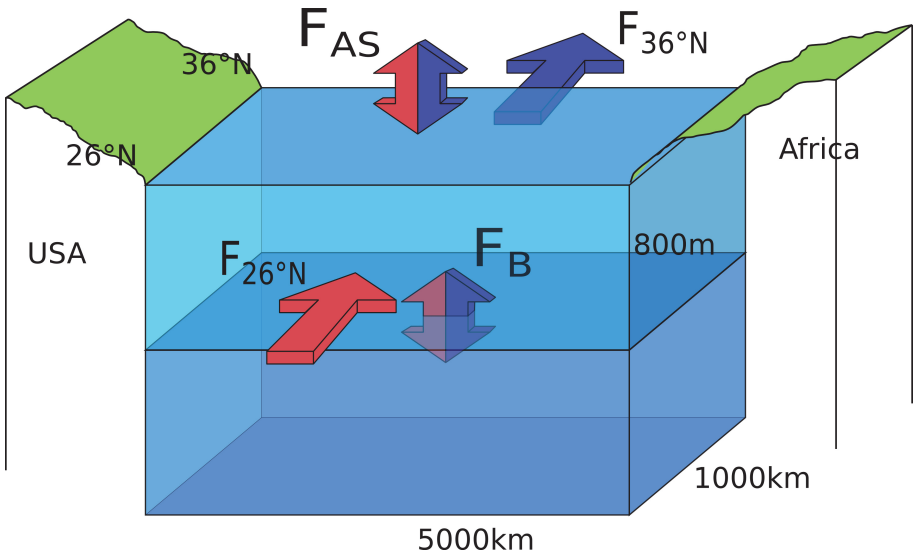

Fig. 1. Sketch illustrating the box model. Red and blue arrows indicate heat flux into and out of the box at 26° N and 36° N, with the sign convention positive into the box. The blue/red arrows represents the air-sea surface flux and the mixing at the interface. There are no fluxes through the eastern and western sides.

OSD
10, 27–53, 2013

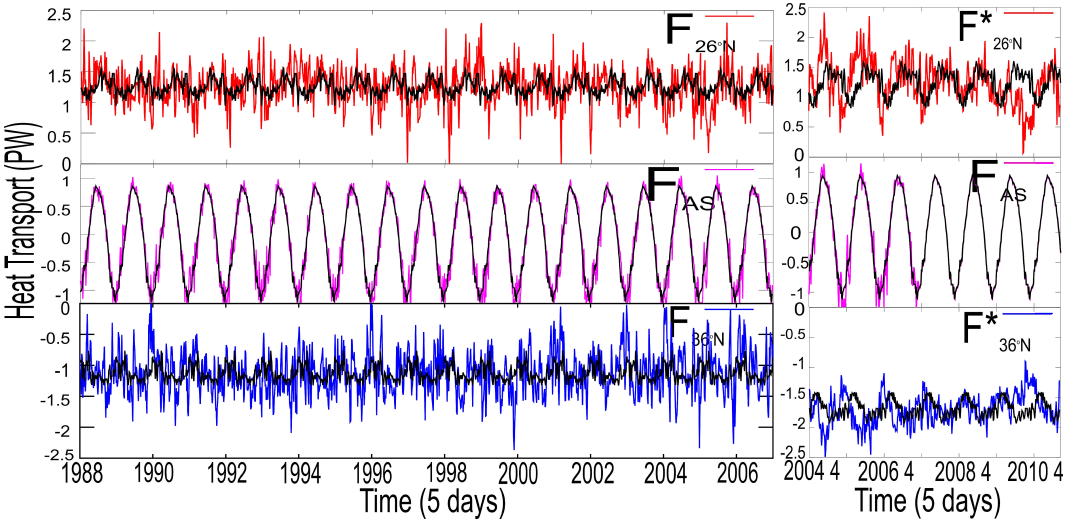

Fig. 2. The MHT (PW) used to force the box model, for AV (left) and FV (right) experiments. Positive (red) transports are entering the box at 26° N, while negative transports (blue) are leaving the box at 36° N. The air-sea flux (air-sea, magenta) can be positive or negative. Black lines illustrate the mean seasonal components of the respective forcing. For the air-sea component for the observational case, the OCCAM derived NCAR forcing was used up to December 2006, and a climatology after that.

OSD
10, 27–53, 2013

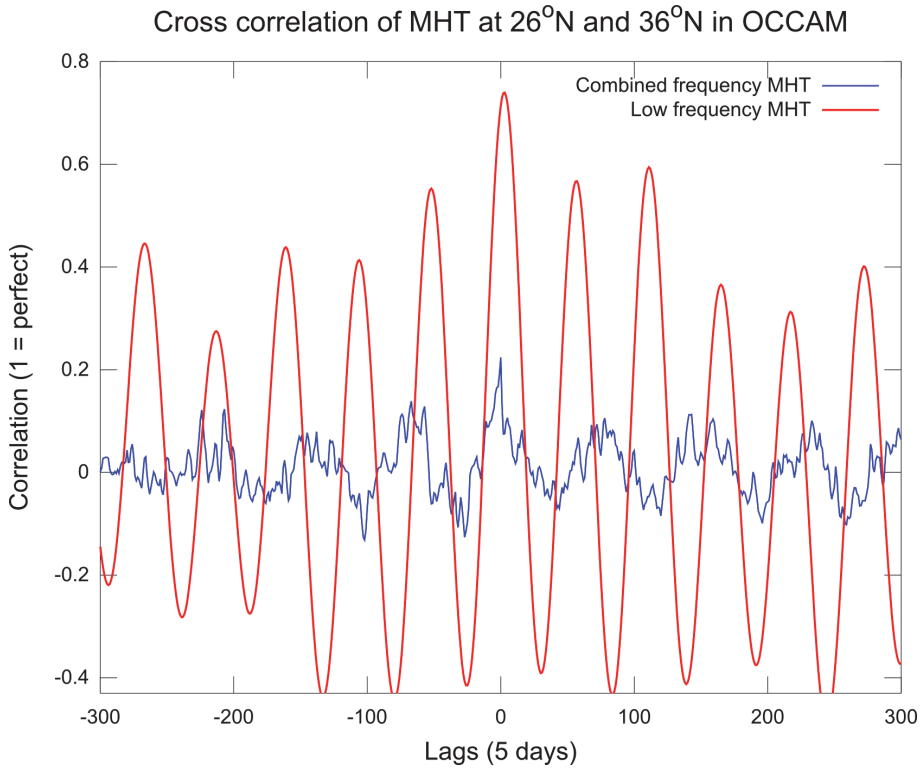

Fig. 3. Figure illustrating the change in cross correlation investigating the full (combined, blue) and the low frequency (red) heat flux $F_{26^\circ\mathrm{N}}$ and $F_{26^\circ\mathrm{N}}$. To seperate the high and low frequency transport a lowpass filter was used. Here the cut-off frequency of 100 days was used, as a marked decrease in the variance of both $F_{26^\circ\mathrm{N}}$ and $F_{26^\circ\mathrm{N}}$ was observed using this.

OSD
10, 27–53, 2013

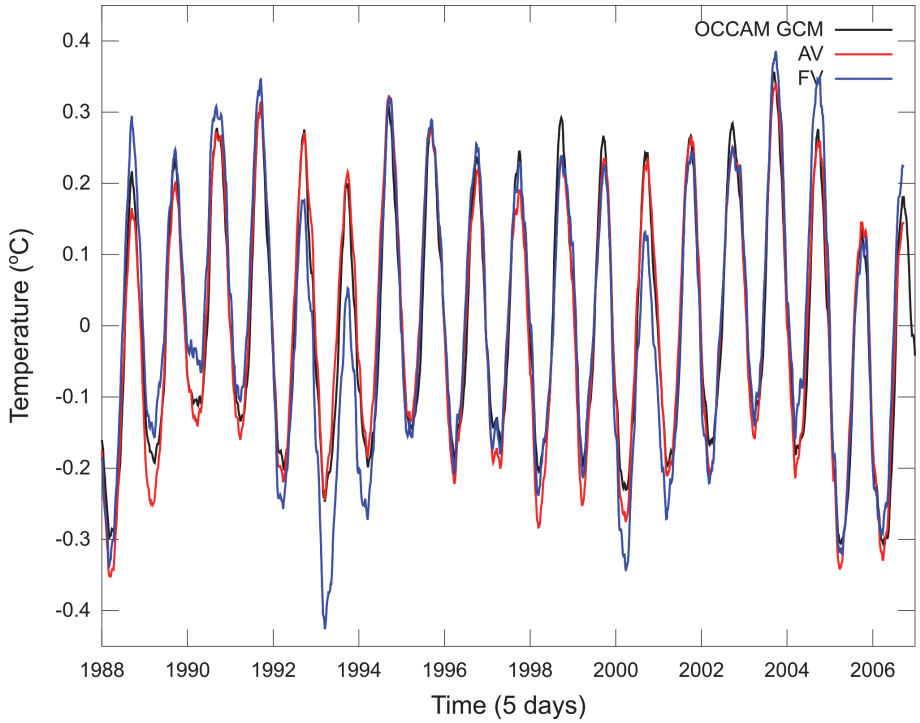

Fig. 4. Demonstration of box model skill, OHC detrended and with the mean removed. Blue line is from the full OCCAM model, red line from the box model AV and black line from the box model FV modified to accommodate observational data, but here run with OCCAM data at 26° N to 36° N. Both box model versions show good agreement with the GCM, and the amplitude of the seasonal signal is well captured.

OSD
10, 27–53, 2013

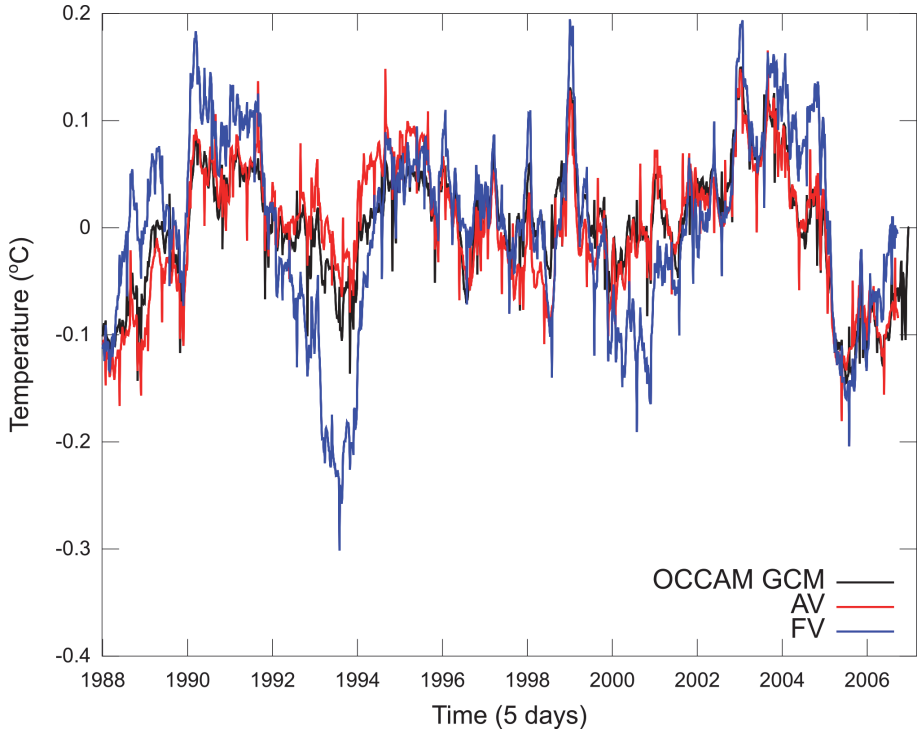

Fig. 5. Interannual detrended temperature variability in the OCCAM model (black) and box model AV (red), FV (blue), all detrended and with the mean removed. The first box model interannual HC median deviation from the OCCAM model of -7.7×10^{-3} °C (standard deviation: 5.7×10^{-2} °C), and the FV box model 2.4×10^{-2} °C (standard deviation: 0.1 °C). This confirms that the box model can be used to investigate the sub- and interannual components of the oceanic and air-sea causes of HC variability.

OSD
10, 27–53, 2013

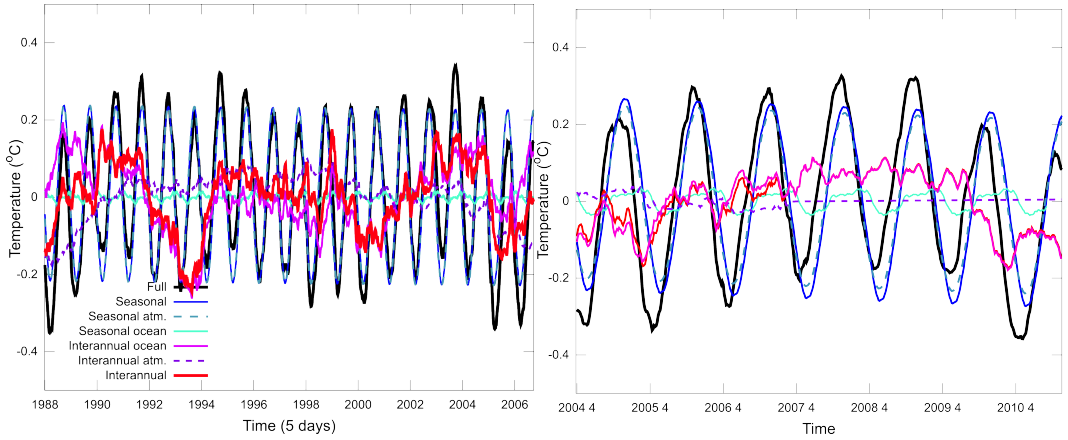

(a) Box Model, AV

(b) Box Model, FV

Fig. 6. Figure summarizing the box model results, detrended and with the mean removed. Right figure shows box model temperature evolution with RAPID MHT at 26° N, inferred MHT at 36° N and air-sea flux from OCCAM. Left figure shows the results with OCCAM forcing at 26° N and 36° N, and OCCAM air-sea flux. Both figures illustrate the OHC variability attributable to the tested forcing scenarios. Note the atmospheric dominance on the seasonal OHC variability, and the oceanic dominance of the interannual OHC variability.

OSD
10, 27–53, 2013

Interannual subtropical North Atlantic heat content variability

M. Sonnewald et al.

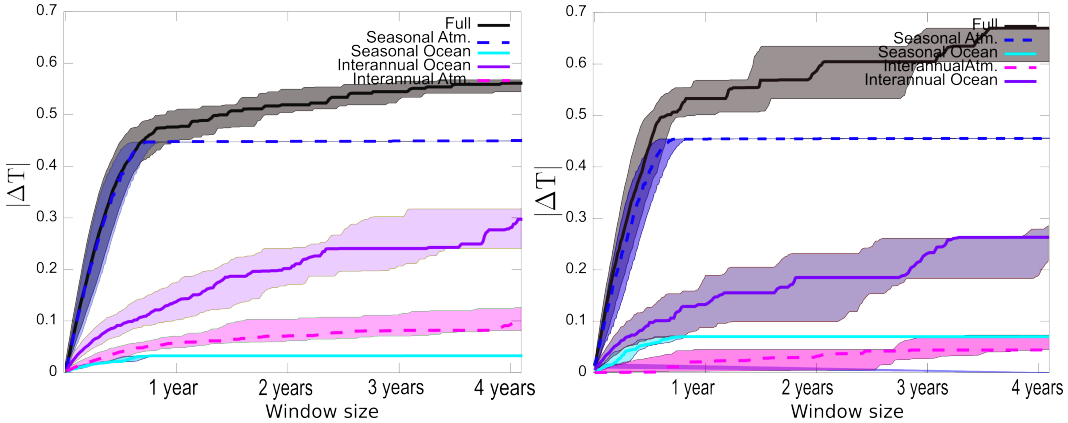

Fig. 7. The absolute magnitude of OHC change ($|\Delta T|$ in $^{\circ}$C) attributed to each component. Coloured regions illustrate the respective first quartile (upper line), median (thick line) and third quartile (lower line) of the largest ΔT within a sliding window of an increasing size. Note the seasonal components stabilise within a year, while the importance of the interannual components increase with time/window size. Further, the figure highlights the partitioning of the importance of the components, illustrating the magnitude of the interannual component, and the timescales this works over.

OSD
10, 27–53, 2013

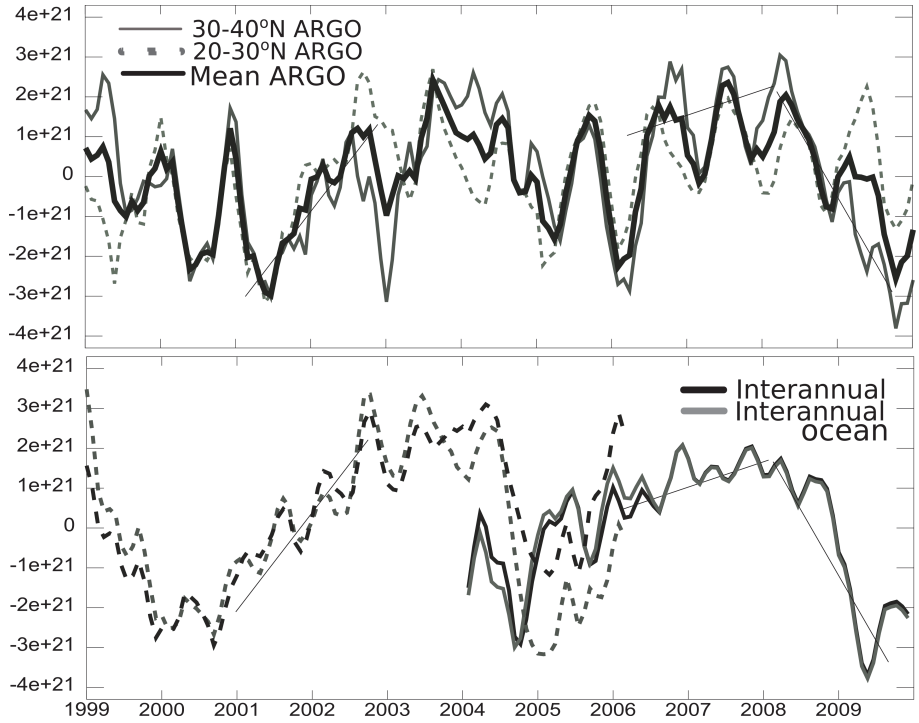

Fig. 8. Top panel showing ARGO derived interannual OHC anomaly with the mean removed (top plot) for the subtropical North Atlantic from 20 to 30° N (solid) and 30 to 40° N (stippled), and the average (thick solid). This is comparable to OHC anomalies from this study shown in the lower panel for the combined (grey) and ocean only (black) for the box model AV (stippled) and FV (solid). Data was smoothed using an S-Golay filter. Note that the event in December 2009 coincides with a period where the 30 to 40° N OHC anomaly was smaller than that at 20 to 30° N, representing a reversal of the dominant situation.

OSD
10, 27–53, 2013